Journal of Structural Geology, Vol. 14, No. 6, pp. 669 to 688, 1992
Printed in Great Britain

0191-8141/92 $05.00+0.00

Structural–metamorphic evolution of the Tia Complex, New England fold belt; thermal overprint of an accretion–subduction complex in a compressional back-arc setting

PAUL H. G. M. DIRKS,* MARTIN HAND,† WILLIAM J. COLLINS and ROBIN OFFLER

Department of Geology, University of Newcastle, NSW 2308, Australia

(*Received* 4 *April* 1991; *accepted in revised form* 18 *November* 1991)

Abstract—Rocks in the Tia Complex underwent a simple, clockwise *P–T–t*-deformation path, moving from mid-crustal levels at blueschist facies conditions (D_1, D_2; 6 kbar, 200°C) to upper-crustal levels at high-*T* amphibolite facies conditions (D_4, D_5; 2.5 kbar, 600°C), in a relatively short time (~15 Ma). The rocks remained under these conditions for approximately 40 Ma (D_6) before they cooled and were brought to the surface (D_7, D_8). During D_6, Permian rift basins were opening as thermal gradients in the Tia Complex reached a maximum.

D_{1-2} deformation was associated with accretion–subduction processes and was followed by progressively less intense, mainly E–W oriented compression and uplift during D_{3-5}, bringing the rocks to within 2 kbars of the surface. D_6 is characterized by limited extensional deformation, and final uplift took place during D_{7-8} along shear zones that have orientations similar to D_{3-5} thrusts.

The shift from subduction-dominated processes to thermally-dominated processes occurred during D_{3-4} uplift of ~4 kbar, around 310–300 Ma. This coincided with a change in tectonic setting of the Tia Complex from an accretionary prism to a back-arc position, as the subduction zone stepped eastward. An increased heat flow, associated with back-arc processes, gradually caused thermal weakening of the lithosphere, which, due to external, subduction-related, compressive forces, resulted in uplift (D_3). With continued heating of the crust, thermal doming resulted and uplift stopped (D_{4-5}), whilst thermal weakening led to limited crustal collapse as Permian basins opened (D_6).

The extremely high heat flow that was maintained for ~40 Ma, suggests a heat source external to the crust, possibly associated with thermal relaxation, dehydration and detachment of the remnant slab left beneath the New England Orogen after the subduction zone shifted east. A stable crustal, thermal structure was re-established by 260 Ma, as the crust strengthened and could further support subduction-induced, compressional structures (D_{7-8}).

INTRODUCTION

THE dominantly Devonian to Carboniferous, southern New England fold belt (NEFB) can be subdivided into the deformed, fore-arc basin associations belonging to the Tamworth Belt in the west, and the accretion–subduction associations belonging to the Tablelands Complex in the east (Fig. 1) (Korsch 1977, Cawood & Leitch 1985, Cross *et al.* 1987). Although the southern NEFB resembles a typical subduction-related orogen, characterized by multiply deformed, imbricate fault slices that underwent low-temperature metamorphism at high to medium pressures with a clockwise *P–T–t* path, there have been an increasing number of recordings of a second regional, high-temperature, low-pressure (high-*T*, low-*P*) metamorphic event that has affected parts of the fold belt whilst a compressional tectonic setting, possibly related to the subduction process, was maintained (Korsch 1977, Vernon 1982, Hand 1988a, Farrell 1988). Effects of this thermal event are exposed in the fault-bounded, high-grade blocks at Tia (Fig. 1) (Gunthorpe 1970, Hand 1988a) and Wongwibinda (Fig. 1) (Binns 1966, Farrell 1988); the latter contains evidence for a regional, anticlockwise *P–T–t* path (Vernon 1982).

It is relatively uncommon for a compressional accretion–subduction terrain to change its metamorphic 'affinity' from high-*P* metamorphism to high-*T* metamorphism, and the tectonic processes that must have operated to accommodate this shift are not well understood. Murray *et al.* (1987) and Hand (1988a) suggested that subduction of a spreading zone may have occurred during the development of the NEFB. A different explanation is given by Harrington & Korsch (1985), who suggested that an eastward shift of the volcanic arc placed the accretion–subduction terrains in an extension-related, back-arc setting. The only well-documented example of high heat flow overprinting high-*P* assemblages in an accretionary terrain has been recorded in the Chugach metamorphic complex of southern Alaska (Sisson & Hollister 1988), where the high thermal gradients are explained to result from tectonic focusing of hot fluids, possibly associated with subduction of young, relatively hot, oceanic crust.

To understand the tectonic processes that operated during the Devonian, Carboniferous and Permian in the southern NEFB, detailed structural–metamorphic analyses of the high-*T* terrains are required. The Tia Complex is especially suited for this, because seemingly coherent rock sequences record high-*P*, low-*T* assem-

*Present address: Institute of Earth Sciences, University of Utrecht, 3508 TA Utrecht, The Netherlands.
†Present address: Department of Geology, University of Melbourne, Parkville, Victoria 3052, Australia.

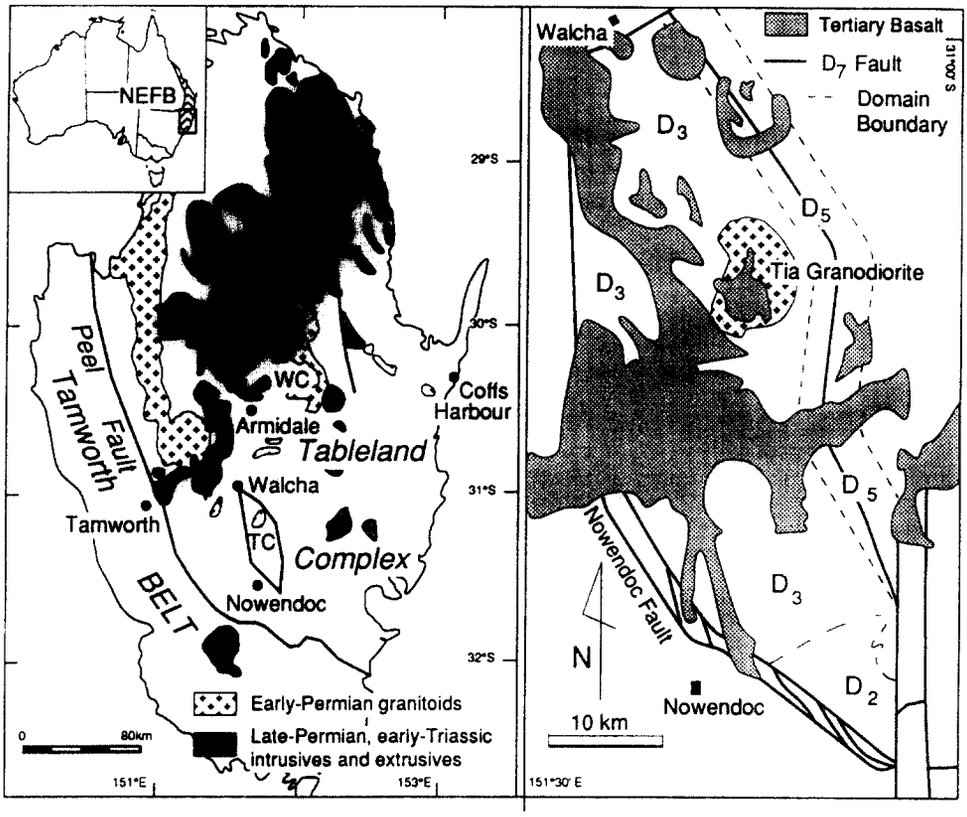

Fig. 1. Map of the southern New England fold belt. Early Permian granitoids belonging to the Hillgrove Suite and related Bundara Suite are indicated. TC = Tia Complex, WC = Wongwibinda Complex. The enlargement shows the Tia Complex, the position of the Tia Granodiorite and the domains in which the three tectonic fabrics, S_2, S_3 and S_5 are the dominant foliations in outcrop.

blages overprinted by regional metamorphic high-T, low-P assemblages (Hand 1988a,b).

In this paper, a structural framework is presented for the complicated, multi-phase fabrics and fold geometries in the Tia Complex. By relating the fabrics with the bimodal metamorphic assemblages and using kinematic indicators, an attempt is made to constrain the P–T–t-deformation path, and in doing so, explain the tectonic processes that operated in the southern NEFB during the late-Carboniferous and Permian.

REGIONAL GEOLOGICAL SETTING

The Tia Complex is situated in the western part of the Tableland Complex of the southern NEFB (Fig. 1) (Runnegar 1974, Korsch 1977). It consists of a series of multiply deformed, poly-metamorphosed rocks intruded by the Tia Granodiorite (Gunthorpe 1970). Reverse shear zones separate the complex from unmetamorphosed Permian sediments of the Manning Basin to the south and southwest, and from relatively weakly deformed, low-grade slate, greywacke and quartzite to the east, north and northwest.

Rocks in the Tia Complex comprise siliceous schist, metagreywacke, metasiltstone, slate, pebbly metapelite, metabasite, chert and jasper beds, serpentinite, and granodiorite, which were subdivided by Gunthorpe (1970) into the more basic and chert-rich Oxley and Wybeena Metamorphics, the pelitic Brackendale Metamorphics, the Nowendoc Ultrabasic Belt and the intrusive Tia Granodiorite. The former two were considered by Korsch (1977) to belong to the Sandon Association, whereas the Brackendale Metamorphics were interpreted as part of the Coffs Harbour Association. The Tia Granodiorite forms part of the Hillgrove Suite, which consists of S-type plutons with low initial $^{87}Sr/^{86}Sr$ ratios, that are interpreted to have been derived from volcanoclastic metasediments (Flood & Shaw 1977, Shaw & Flood 1981).

Although Gunthorpe (1970) believed that the four lithostratigraphic units occurred in distinct, fault-bounded blocks, the lithological transitions appear gradual. In general, rocks in the western half of the Tia Complex consist predominantly of metapsammite and metapelite, whereas to the east and southeast, the metabasite, chert and jasper components increase dramatically, and are dominant in the Nowendoc area (e.g. Hand 1988a). Serpentinite is restricted to the southernmost part of the complex, where it appears partly intercalated with the mafic rocks and parallels the bounding shear zone: the Nowendoc Fault.

Regional metamorphic assemblages in the area can be subdivided into two major assemblage groups: the first comprising sodic amphibole–actinolite–pumpellyite–albite–chlorite–phengite, and the second containing hornblende–plagioclase (metabasite) and biotite–

muscovite–garnet (metapelite). The former is associated with high-P, low-T metamorphism and occurs exclusively in the southern section of the Tia Complex (Gunthorpe 1970, Hand 1988a). The latter is associated with high-T, low-P metamorphism (Hand 1988a) and is spatially associated with the Tia Granodiorite. Gunthorpe (1970) suggested that the high-T assemblages resulted from emplacement of the granodiorite, and thought that after emplacement, the terrain cooled and was buried to form the blueschist. However, Hand (1988a,b) showed the contrary to be true for the Nowendoc area where high-T, low-P assemblages overprinted high-P, low-T assemblages.

The structural development of the Tia Complex is extremely complicated, and little published information is available on the exact nature of the various overprinting fabrics. Gunthorpe (1970) recognized three regionally significant folding events, but did not correlate these with specific metamorphic assemblages, or kinematic interpretations. Hand (1988a,b) recognized six folding events that are associated with particular mineral fabrics near Nowendoc (Fig. 1). The earliest two fabrics formed under blueschist facies conditions and were folded by F_3 folds containing axial planar, transitional blueschist–greenschist facies assemblages. These were, in turn, refolded by two or three folding events that took place at greenschist facies grade. Hand (1988a) noted that the transition from blueschist to greenschist facies was paralleled by the development of D_3 shear zones.

In this paper the basic structural outline as proposed by Hand (1988b) has been extended to include folding and faulting episodes that exist beyond the Nowendoc area. It will be shown that the intensities of the different fold episodes and related fabrics varies considerably throughout the area, making it impossible to recognize all folding events in each part of the complex.

MACRO- AND MESOSCOPIC STRUCTURAL FRAMEWORK OF THE TIA COMPLEX

Eight overprinting deformation events can be recognized, which include the fabric-forming folding events F_1–F_5, a non-fabric-forming folding event F_6, a ductile shearing event D_7, and a brittle faulting event D_8. Only D_3 and D_5, as S_3 and S_5, can be traced continuously throughout the Tia Complex, and were used as 'reference foliations' to correlate the other deformational events. There are a number of form surfaces defined by different foliations, each of which locally constitutes the dominant foliation in outcrop. In general, the form surface in the Tia Complex is defined by S_2 in the south, S_5 along the western boundary, and S_3 in the rest of the area (Fig. 1). Transitions from one form surface to the next result from progressive transposition of the earlier foliation (e.g. S_3) into the later one (e.g. S_5). Apart from rare individual outcrops, S_1 and S_4 never become the dominant foliation.

D_1 *deformation*

Effects of D_1 include early veining, disrupted bedding, tectonic melanges and a locally developed S_1 fabric, which are best preserved in the southern part of the complex. None of the D_1 features is penetrative and all have been transposed into S_2 making their identification and orientation determination difficult; it is possible that pre-S_2 fabrics formed during several deformational events.

The penetrative S_2 foliation usually wraps around 0.1–50 cm long, asymmetrical, lenticular fragments or phacoids of competent material, usually chert, jasper, milky vein quartz, quartzite, arkose or metabasalt. These fragments make up a melange in which bedding and stratigraphy are strongly disrupted. The melange is transected by numerous quartz–epidote veins that are isoclinally folded within S_2, indicating that the brecciation process was pre-D_2. Individual fragments may contain an internal, spaced, differentiated, white mica foliation which is truncated by S_2 at the boundary of the fragments and is therefore referred to as S_1.

D_2 *deformation*

The southwest corner of the Tia Complex is dominated by a penetrative S_2 foliation which generally dips moderately to the southwest (Fig. 2). Macroscopic F_2 folding has not been identified, however, mesoscopic F_2 folds with an axial planar S_2 foliation are abundant, and are outlined by bedding and D_1 veins. Such folds are generally tight to isoclinal and have a maximum wavelength of about 1 m. F_2 fold axes and a mineral elongation lineation, L_{2x}, are parallel and generally plunge 20–30° to 230–240°.

The S_2 foliation and L_{2x} elongation lineation in quartzitic schist are defined by a mm- to cm-scale, lenticular, compositional layering that consists of flattened and elongated fragments of chert and quartzite, embedded in a schistose matrix of aligned white mica and chlorite. S_2 within metabasite units is more regular and defined by alternating epidote-rich layers (5–10 mm thick) and layers dominated by chlorite and actinolite, which also define L_{2x}.

Where S_2 is strongly developed it becomes mylonitic and is associated with S–C fabrics, shear bands and asymmetric phacoids which occur in 'stepped up' arrangements similar to 'bookshelf sliding' described by Ramsay & Huber (1987), all of which indicate a top-to-the-SW normal sense of movement. S_2 is transposed in S_3 in a 1 km wide transition zone in which it becomes progressively more intensely folded in F_3 and overprinted by S_3 and L_{3x} (Fig. 2). North of this boundary zone, S_2 is only preserved along the hinge regions of F_3 intrafolial folds.

D_3 *deformation*

S_3 is the dominant foliation throughout much of the Tia Complex (Figs. 1 and 3) and is generally associated

with a penetrative mineral stretching lineation L_{3x}. In the western section of the complex, where all later deformations were less intense (Figs. 4, 5 and 6), S_3 and L_{3x} generally dip/plunge to the west or southwest at moderate angles (Fig. 7). L_{3x} remains in this orientation when D_3 fabrics are only affected by macroscopic F_4 folds (e.g. east of Nowendoc, Fig. 3). Where macroscopic F_5 folding becomes significant, S_3 and L_{3x} are variable (e.g. directly south of the Tia Granodiorite, Fig. 3).

Where S_3 is the form surface, macroscopic F_3 folding is absent; mesoscopic folds are rare in the north, but become increasingly common towards the Nowendoc area where the D_3 overprint of S_2 is less intense. As a consequence, F_3 folds in the north are mainly defined by isoclinally folded quartz veins whereas further south, transposed fold hinges defined by S_2 are more common. All F_3 folds have fold axes that are generally closely parallel to L_{3x} and a number of folded quartz veins display sheath-like geometries suggesting high strain as a result of non-coaxial flow (Cobbold & Quinquis 1980).

East of Nowendoc, S_2 forms macroscopic F_3–F_4, 'dome and basin'-type interference folds (Fig. 2) (Hand 1988b). If F_4 effects are removed, a single, NE-verging, reclined, tight F_3 antiform remains with a wavelength of at least 5 km and a fold axis that plunges moderately to the westnorthwest, parallel to most of the mesoscopic F_3 fold axes in this area, and at a moderate angle to L_{3x} (Fig. 3) (Hand 1988b). The overturned lower limb of this fold is transposed into S_3 towards the northeast.

In the southern part of the complex, S_3 is generally only developed in mica schist in the hinges of mesoscopic F_3 folds, where it occurs as a zonal crenulation cleavage (Gray 1977), locally becoming a continuous schistosity. Elsewhere, S_3 and L_{3x} are very strongly developed and outlined by aligned mica or amphibole grains and quartz rodding (Fig. 8a), commonly parallel to a mm-scale, differential layering, which is planar and regular, giving the rock a gneissic appearance. Many of the lenses are quartzitic or cherty in composition and probably resulted from continued straining of the phacoidal fabrics and quartz veins produced during D_1 and D_2. Locally, polymict conglomerate units contain stretched pebbles, elongated along L_{3x} (e.g. granite pebbles at GR 7455780; grid references refer to the 1:100,000 topographic map sheet 'Yarrowitch').

The S_3 foliation generally shows a clear asymmetry in sections parallel to L_{3x}, with S–C fabrics transected by shear bands, clasts with asymmetric pressure shadow tails and micro-folds, all of which indicate a SW-over-NE sense of movement.

D_4 *deformation*

D_4 effects are restricted to the central and southeastern half of the Tia Complex (Fig. 5) and are associated with E–W-trending, open to tight, rounded to subrounded, upright folds (class 1c, Ramsay 1967) with wavelengths of up to 6 km (Figs. 4 and 5). In the south, F_4 folds deform S_2 and overprint F_3 folds of similar scale, resulting in characteristic 'dome and basin' structures (Fig. 2). Elsewhere, F_4 folds deform S_3 and are generally the earliest recognizable folds in outcrop.

F_4 folds are associated with a discrete, axial planar crenulation cleavage in which metamorphic differentiation and new growth of mica and amphibole grains has taken place to define S_4 (Fig. 8b). In the south, S_4 is mainly defined by muscovite in mica schist and chlorite–actinolite in metabasite, whereas further north, biotite and hornblende are dominant. Usually S_4 is enhanced by seams of opaques that resulted from solution transfer of soluble material away from the cleavage planes. Mineral elongation lineations or asymmetrical features within S_4 are almost completely absent, and the largest-scale F_4 folds are essentially symmetrical (Fig. 4).

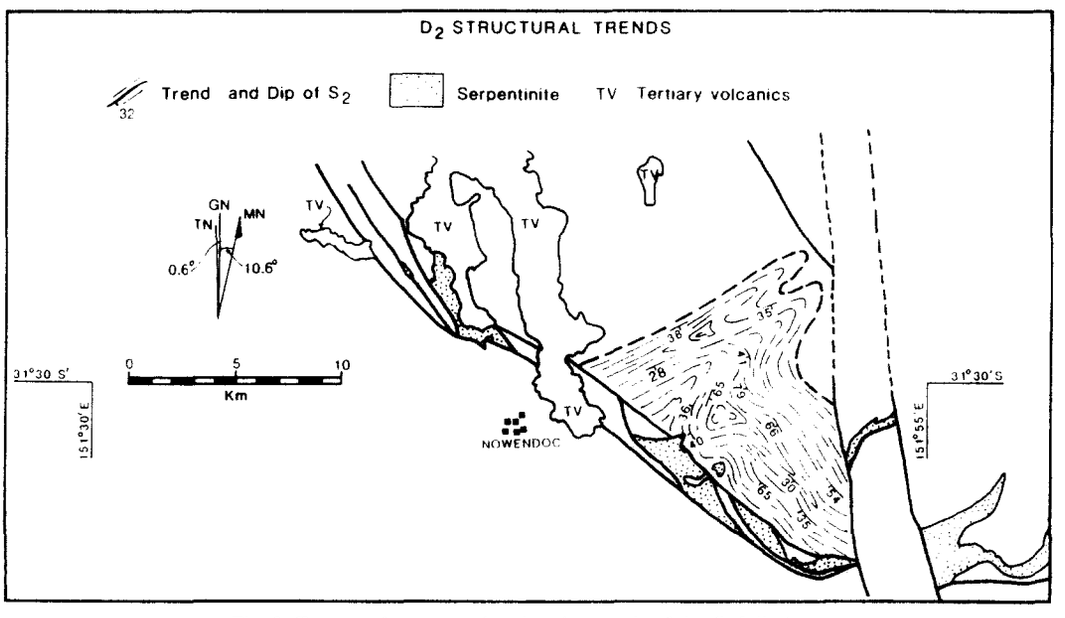

Fig. 2. Form surface map, showing the trends of the S_2 foliation.

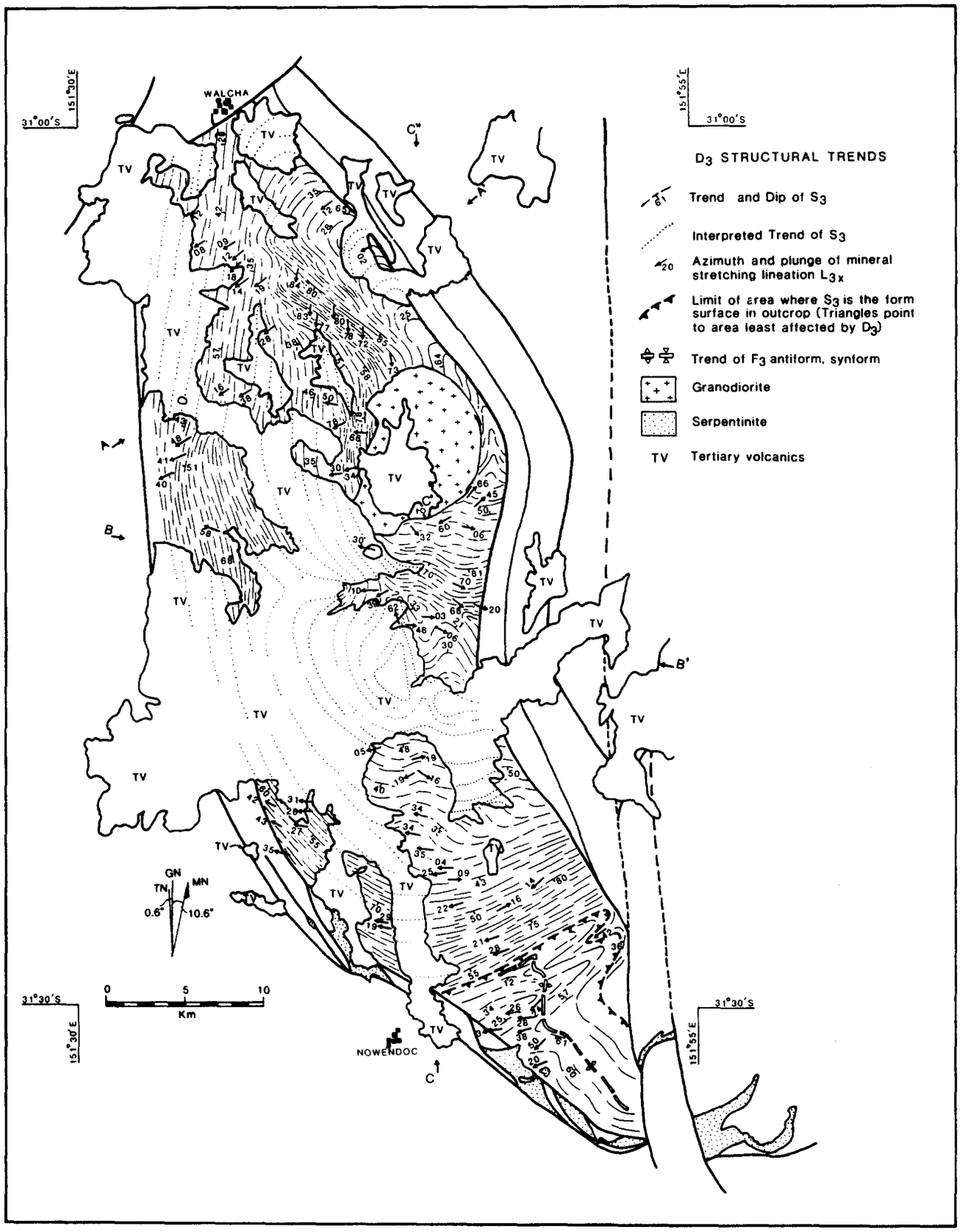

Fig. 3. Form surface map, showing the trends of the S_3 foliation.

Although F_4 folds are commonly overprinted by F_5 folds of similar scale, S_4 generally remains planar (Figs. 4 and 5). This is apparent on every scale, and is directly reflected in stereoplots of S_4 (Fig. 9). Its significance will be discussed with D_5 deformation. In general, S_4 is subvertical, trends east and varies slightly as a result of F_6 folding, whereas F_4 fold axes (L_4) are variable within S_4 due to F_5 folding (Fig. 9). In outcrop, L_4 almost invariably parallels L_{3x} which seems to suggest a genetic relationship between D_3 and D_4.

D_5 *deformation*

D_5 is the last penetrative deformation in the Tia Complex, and its effects are best preserved. Going east, D_5 structures gradually increase in intensity and culminate in a 5 km wide shear zone at the eastern boundary of the complex where S_5 is the form surface (Figs. 4 and 6). Other syn-D_5 events include the emplacement of the Tia Granodiorite (Dirks *et al.* in press a), aplite dykes and numerous quartz veins.

On the basis of the D_5 intensity, four domains may be distinguished (Fig. 10). Domain 1 occurs along the western boundary of the Tia Complex and lacks macroscopic F_5 folding and a penetrative S_5 foliation. Domain 2 is characterized by abundant F_5 folding, both mesoscopic and macroscopic, and a generally penetrative, but

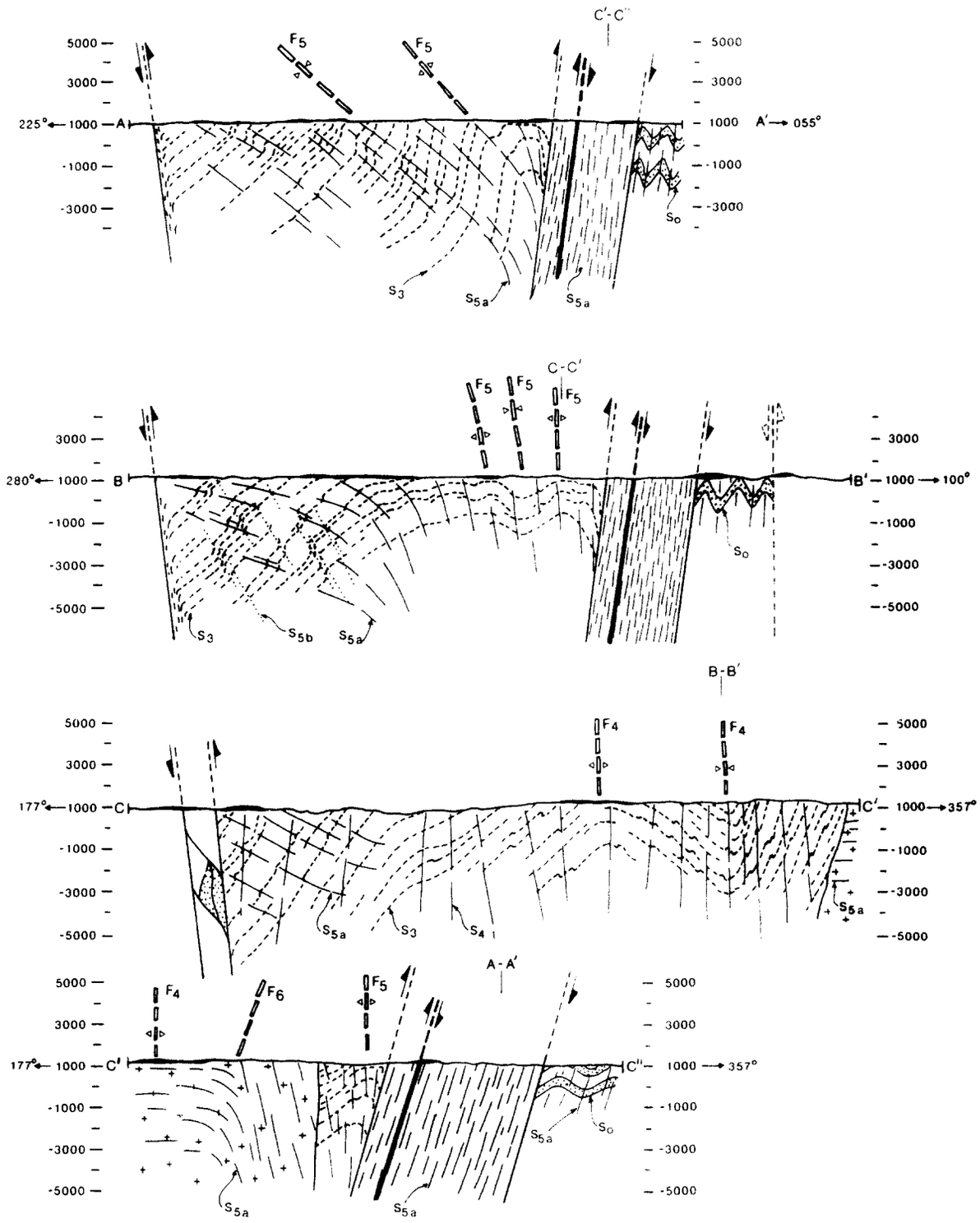

Fig. 4. Structural profiles through the Tia Complex as indicated in Fig. 3. The principal foliations shown in the profiles are S_3 and S_5 which have been labelled accordingly. Two coeval S_5 foliations could be recognized in the western Tia Complex; a dominant S_{5a} foliation and locally developed S_{5b} foliation (see text for further discussion). The dip of the fault at the western boundary of the complex is unknown, as the fault was not observed in outcrop. Its position has been estimated from fracture cleavages that have developed in its vicinity.

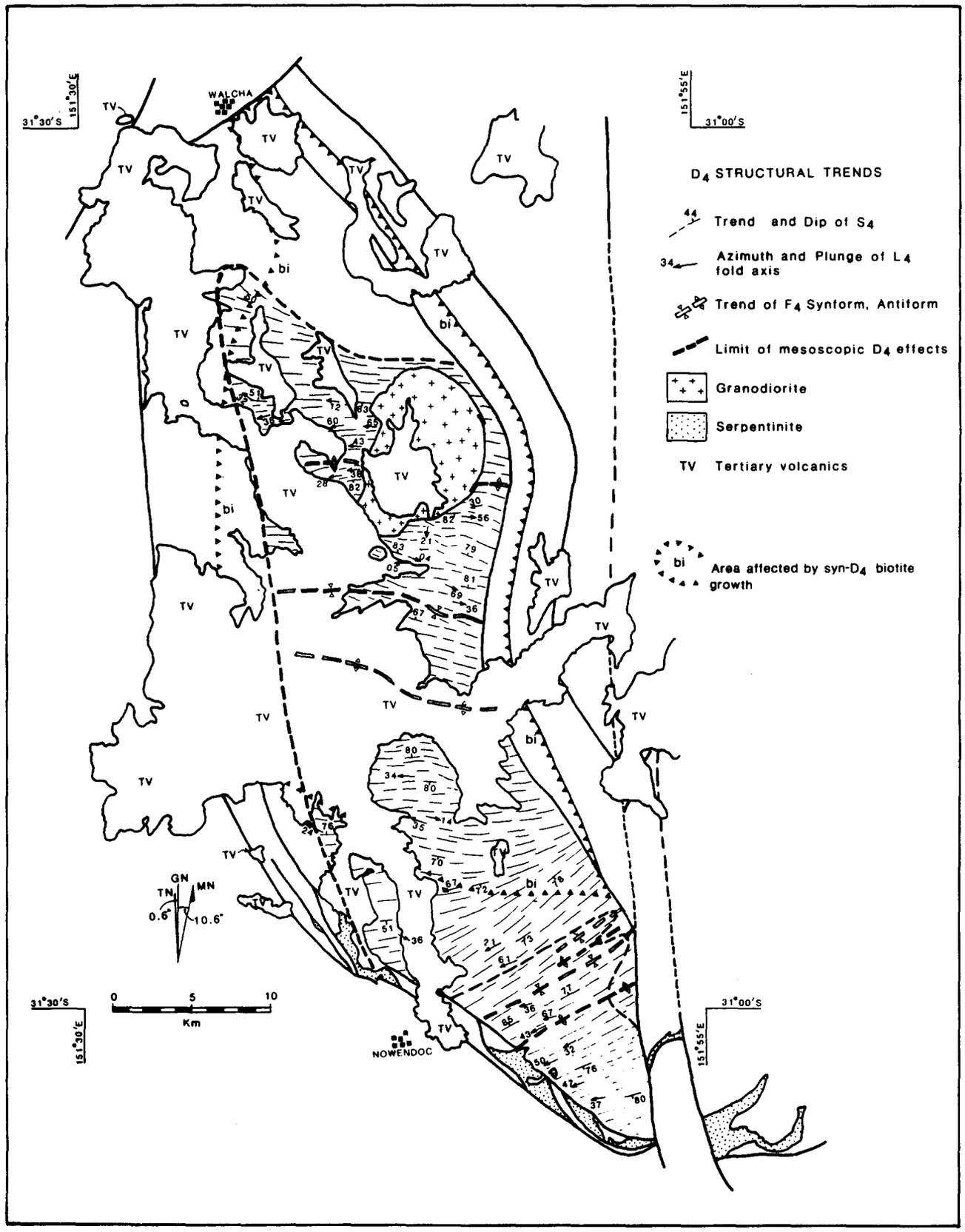

Fig. 5. Form surface map, showing the trends of the S_4 foliation. The position of the D_4 biotite isograd was based on thin section work and reinterpretation of data collected by Gunthorpe (1970).

not dominant, S_5 foliation. In Domain 3, S_5 constitutes the form surface and a mineral elongation lineation, L_{5x}, is strongly developed. Domain 4, completely lies within Domain 2 but covers the Tia Granodiorite, which does not display the same intensity of deformation as the surrounding rocks, as it intruded during D_5.

In *Domain 1*, S_5 is only locally developed as a spaced, discrete, solution enhanced crenulation cleavage,

occasionally accompanied by some new growth of mica or amphibole. S_5 dips to the northeast and is axial planar to F_5 folds that are distinctly asymmetrical, verge towards the southwest and have subhorizontal fold axes with a northwest azimuth (Fig. 10). It is common to find two sets of F_5 folds in one outcrop; one shallowly dipping and one steeply dipping, both with the same vergence and fold axis (this has been illustrated in Fig. 4, profile B,

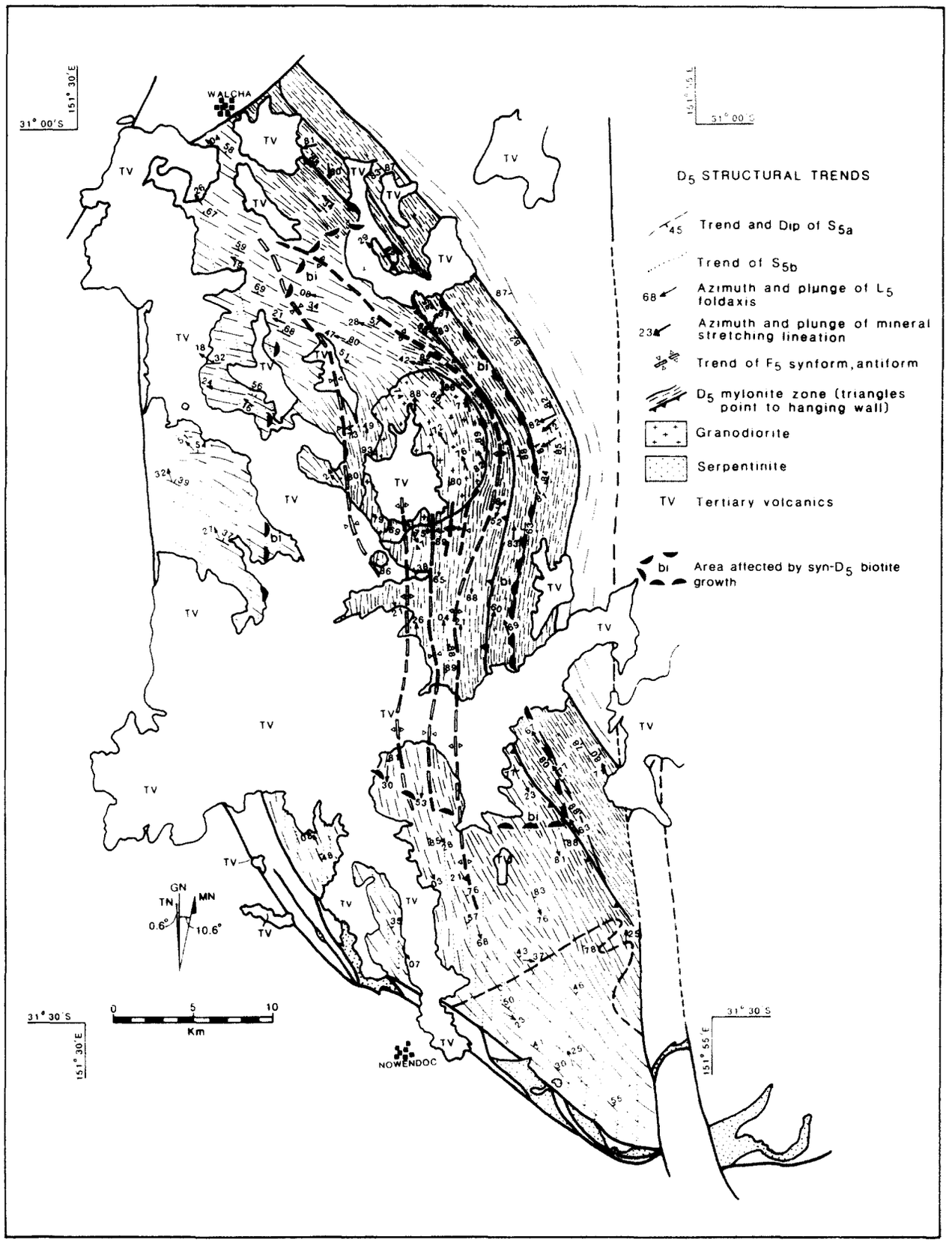

Fig. 6. Form surface map, showing the trends of the S_5 foliation, which generally dips steeply. The density of the drawn trend lines coincides with the observed increase in intensity of D_5 structures. Note that the areal distribution of D_5 biotite is reduced relative to D_4 biotite.

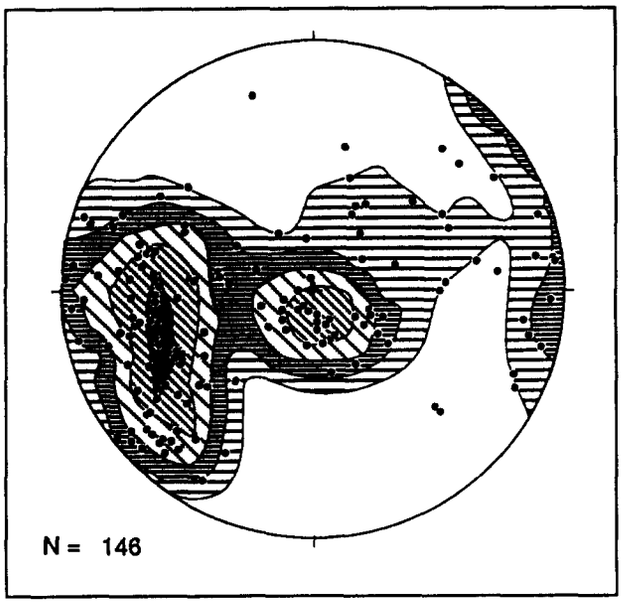

Fig. 7. Equal-area plot, showing both the scatter and contour distribution of L_{3x}. The observed spread away from a general southwest plunge is mainly due to F_5 folding. Contour intervals are 5%.

where they are labelled S_{5a} and S_{5b}), and generated from the same discontinuity in the rock (e.g. a boudin neck), suggesting a progressive development.

In *Domain 2* the intensity of mesoscopic and macroscopic F_5 folding dramatically increases. In general there is only one set of F_5 folds developed, which are upright, open to closed, rounded, symmetrical folds (class 1c, Ramsay 1967) (Fig. 8c) with maximum wavelengths of 2 km (Fig. 6). S_5 dips steeply E to SE, and F_5 fold axes (L_5) are highly variable within S_5 (Fig. 10). The spread of L_5 along two separate great circles (Fig. 10-II) is a result of F_6 folding. The spread of L_5 within S_5 results from F_4–F_5 interference folding and the non-cylindrical nature of high-strain F_5 folds.

Apart from their orientation, F_4 and F_5 folds are indistinguishable in outcrop. In general S_4, L_4, and S_5, L_5 are at high angles, which results in type 1 interference patterns dominated by basins and domes (Ramsay 1967, Thiessen & Means 1980, GR 785430, Fig. 8d). Because S_4 is generally not folded, the D_5 shear direction causing F_5 folding must have been close to the subvertical S_4–S_5 intersection. Pseudo-'dome-and-basin' structures, with no regularly spaced distribution of domes or basins, occur in zones where F_4 folding is absent (e.g. GR 761578) and illustrate the non-cylindrical to sheath-like nature of some of the F_5 folds (more frequently so as Domain 3 is approached).

S_5 is a solution enhanced, discrete crenulation cleavage (Fig. 8b) generally defined by oriented quartz domains, micas, amphiboles and seams of opaques. A subvertical L_{5x} mineral stretching lineation may be present and is defined by rodded quartz or oriented mica flakes.

Other typical structures in Domain 2 include boudin trains in S_3 which have been folded in F_5, and a large number of overprinting quartz veins that generally are subvertical and display progressively more intense F_5 effects as they are offset relative to one another in an anticlockwise sense (viewed within the horizontal, Fig. 8e). Both features illustrate the progressive, non-coaxial nature of D_5 deformation.

In *Domain 3*, S_5 has a N- to NW-striking, subvertical orientation, and contains a well developed, subvertical mineral elongation lineation, L_{5x}, generally defined by quartz rods and mica flakes. F_5 folding of S_3 is only visible on outcrop-scale and is generally sheath-like with L_5 parallel to L_{5x} (Fig. 10). Asymmetrical features in S_5 are common and include asymmetrical micro-folds, *S–C* and *C'* fabrics, all of which indicate a W-over-E sense of movement parallel to L_{5x}.

Domain 4 is restricted to the Tia Granodiorite, which contains a penetrative S_5 foliation defined by stringers of biotite and a quartz grain shape fabric, both of which also define a generally weakly developed L_{5x}. Orientations of S_5 and L_{5x} in the granodiorite are consistent with the surrounding schist in Domain 2 (Fig. 10). The granodiorite was emplaced late syn-D_5 (Dirks *et al.* in press a) because: (1) the granodiorite truncates F_5 folds as the contact itself is mildly folded in the same folds and the axial planar S_5 foliation passes coherently across the contact; (2) schistose xenoliths contain truncated F_5 folds and an internal S_5 foliation which is aligned with S_5 in the granodiorite; and (3) contact metamorphic muscovite clots are oriented in S_5.

In general, D_5 deformation resulted from W-over-E movement on a shear zone along the eastern boundary of the Tia Complex and most of the complex represents the coherent but plastically deformed hanging wall (note drag of S_{5a} in Fig. 4, section A).

D_6 *deformation*

D_6 deformation involved large-scale folding of all previously described foliations, illustrated in Fig. 10(II) which displays two clear orientation concentrations of S_5 and L_5. F_6 folds are angular, vertical folds with a wavelength of 15–20 km and an axial trace that runs E–W (e.g. Fig. 5). In outcrop, very few F_6 effects have been identified, apart from some E–W-trending crenulation zones. Possible D_6 structures include steeply dipping sets of quartz veins, which are commonly parallel to S_5. Marker horizons truncated by the veins are generally offset along an orientation that contains a W-down component, which is opposite to the sense of movement during D_5.

D_7 *deformation*

D_7 is manifested in the Tia Granodiorite as a NNW-trending, steeply E-dipping, foliation, S_7 (Fig. 11), which truncates S_5. Outside the intrusion S_7 is difficult to identify due to its similarity in orientation to S_5. S_7 is a spaced cleavage, outlined by thin seams of opaques and enhanced by new growth of fine-grained biotite and muscovite, which together with quartz rods define a down-dip mineral elongation lineation, L_{7x} (Fig. 11). S_7

is completely lacking in the western half of the Tia Granodiorite, but becomes progressively more intense towards the east. In the microlithons between two S_7 surfaces, S_5 is generally sigmoidal, giving single outcrops a S–C appearance in which S_7 is invariably associated with W-over-E movement. However, S_5 and S_7 are not co-genetic because S_5 in the granodiorite is openly folded in F_6, whereas S_7 is not (Figs. 6 and 11) (Dirks *et al* in press a). The occurrence of biotite and muscovite along S_7, the eastward intensification of S_7, and its non-coaxial nature suggest that D_7 may involve reactivation of the D_5 shear zone at relatively high grades.

D_8 *deformation*

Throughout the Tia Granodiorite, but especially along its eastern margin, numerous subvertical, NNW-trending ultramylonite and pseudotachylyte veins overprint all previous foliations (Fig. 8f). The higher density of these features in the eastern part of the complex suggests they resulted from brittle–ductile reactivation of the D_5 shear zone. The exact position of such a fault has not been identified, but probably coincides with the sudden drop in metamorphic grade to the east that occurs close to the western margin of the D_5 shear zone.

The western boundary of the Tia Complex is the Nowendoc Fault (Gunthorpe 1970), which is probably a D_8 structure. No exposure of the fault has been found, but the schists close to the fault show a distinct fracturing and reorientation (Fig. 4), which overprints F_5 and indicates an E-over-W displacement sense.

MICROSTRUCTURE AND METAMORPHISM

D_1 *deformation*

S_1 generally occurs as remnant foliation traces, transposed into a spaced, S_2 crenulation cleavage. S_1 and S_2 commonly display asymmetric relationships reminiscent of S–C fabrics, suggesting that in many instances they formed coevally or progressively during a D_1–D_2 non-coaxial (subduction) event.

In phacoidal fragments, S_1 is a differentiated foliation defined by phengitic white mica ± epidote in metaquartzitic rocks, and by sodic amphibole, actinolite, epidote and chlorite in metabasite. Matrix minerals include fine-grained (<20 μm) aggregates of quartz and albite, whereas sphene is common in metabasite. Relic, igneous clinopyroxene grains with rims of sodic pyroxene and beards of crossitic sodic amphibole aligned in S_1 are locally preserved in metabasite (sample 13609). Blocky aggregates of albite in one sample (13609), suggest that lawsonite may have been a stable phase during D_1 (Hand 1988a). The mineral assemblages that formed during D_1 are therefore quartz–albite–phengite ± epidote in metasediment, and quartz–albite–crossitic sodic amphibole–actinolite–epidote–chlorite ± jadeitic pyroxene ± lawsonite in metabasite.

D_2 *deformation*

In quartzitic and pelitic schist, S_2 is generally a penetrative foliation defined by fibrous (length <100 μm), phengitic white mica and chlorite crystals set in a matrix of fine-grained, equant (<20 μm) quartz ± albite ± epidote. Locally, in more competent, quartzitic rocks, S_2 is a mm-scale differentiated layering, with alternating bands of quartzite and mica schist and remnants of an earlier, S_1, mica foliation. The strength of the S_2 foliation in metabasite is variable and igneous textures are common. Depending on bulk rock composition (especially Fe^{3+} content), clinopyroxene (Cpx) is either replaced by spongy aggregates of strongly pleochroic pumpellyite (sample 122) or by sodic amphibole (e.g. sample 120), as both mineral phases generally do not occur together. Where S_2 in metabasite is strongly developed, it is generally defined by evenly distributed needles of actinolite (length <300 μm) and to a lesser extent sodic amphibole, with fine-grained (length <100 μm), prismatic to blocky epidote, pumpellyite, chlorite and stilpnomelane in the groundmass. Cpx and D_2 actinolite (e.g. samples 115 and 120) are commonly fragmented and extended in the foliation, and fibrous, crossitic to riebeckitic sodic amphibole or chlorite has grown parallel to S_2 in the cracks and along pressure shadows of individual clasts (Fig. 12a). Therefore, the stable D_2 mineral assemblage in the southern Tia Complex included phengite–chlorite–quartz ± albite ± epidote in metasediments, and sodic amphibole–actinolite–chlorite–stilpnomelane–epidote–quartz–albite, and epidote–actinolite–chlorite–pumpellyite–quartz in metabasic rocks.

D_3 *deformation*

D_3 effects occur throughout the Tia Complex, but mineral assemblages in the northern half have been poorly preserved as a result of D_{4-5} amphibolite facies grade overprint. Where S_3 is the form surface (Fig. 1), the rocks are dominantly metasedimentary, and S_3 consists of a penetrative slaty cleavage defined by fine-grained (length <50 μm) muscovite and chlorite flakes in the south and west, and by slightly coarser-grained (length <300 μm) biotite, muscovite ± chlorite elsewhere. The first appearance of D_3 biotite coincides with the first appearance of D_4 biotite as shown in Fig. 5. Although S_3 is generally an even-layered, homogeneous foliation, it locally contains clear mylonitic characteristics, most notably asymmetric, recrystallized tails of quartz on chert fragments (Fig. 12b). These clasts are generally of a σ-type (Passchier & Simpson 1986), suggesting that the rotation rate of the clast was low relative to the recrystallization rate. In metabasite in the higher-grade areas (e.g. sample 88, GR 798267), S_3 is defined by accicular aggregates of pale blue–green hornblende with less common brown biotite. Outside the biotite zone for metapelite, S_3 is defined by accicular actinolite, chlorite ± green biotite which occurs in a matrix of epidote, quartz and chlorite. Locally (e.g.

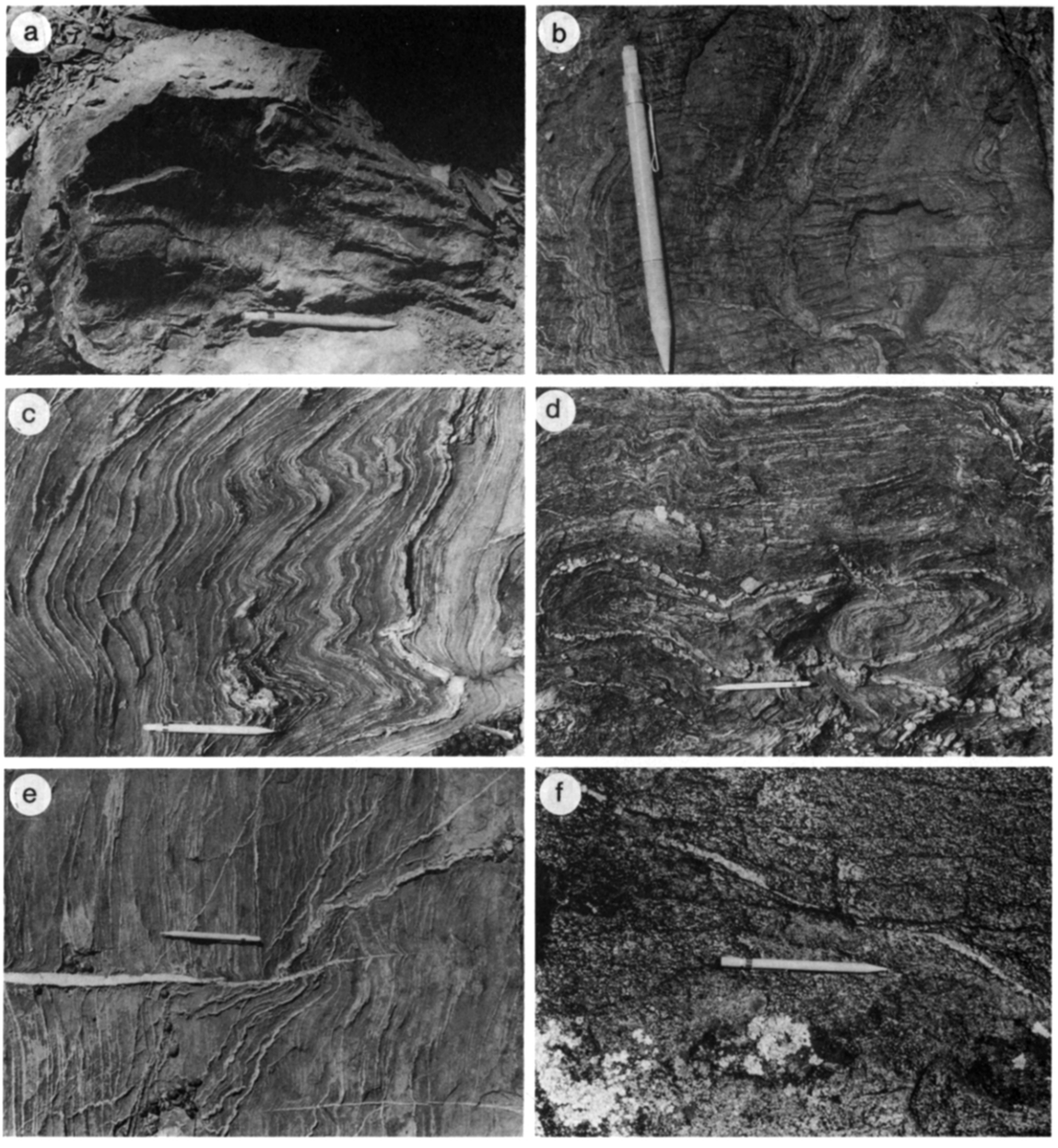

Fig. 8. Mesoscopic structures; the pencil used for scale is 15 cm long. Apart from photograph (a) all other photographs were taken on horizontal surfaces. (a) A S_3 foliation containing a strongly developed L_{3x} defined by rodded quartz grains are folded in F_5 (GR 778388). (b) F_4 folding with a typical, discrete, axial planar, S_4, crenulation cleavage defined by metamorphic differentiation and new growth of biotite (GR 742558). Within isolation, this foliation is indistinguishable from S_5 apart from the fact that its orientation is E–W. (c) Typical, open to closed, rounded, symmetrical F_5 folds belonging to class 1c of Ramsay (1967, GR 810402). (d) 'Dome-and-basin' type, F_4–F_5, interference folding (GR 806455). (e) Several generations of syn-D_5 quartz veins which are progressively folded and rotated in an anticlockwise sense illustrating the progressive, non-coaxial nature of D_5. (f) A thin D_8 ultramylonite band, parallel S_7 in the granodiorite, offsets a syn-D_5 quartz veinlet in a sinistral, top-of-photograph-up sense (GR 824514).

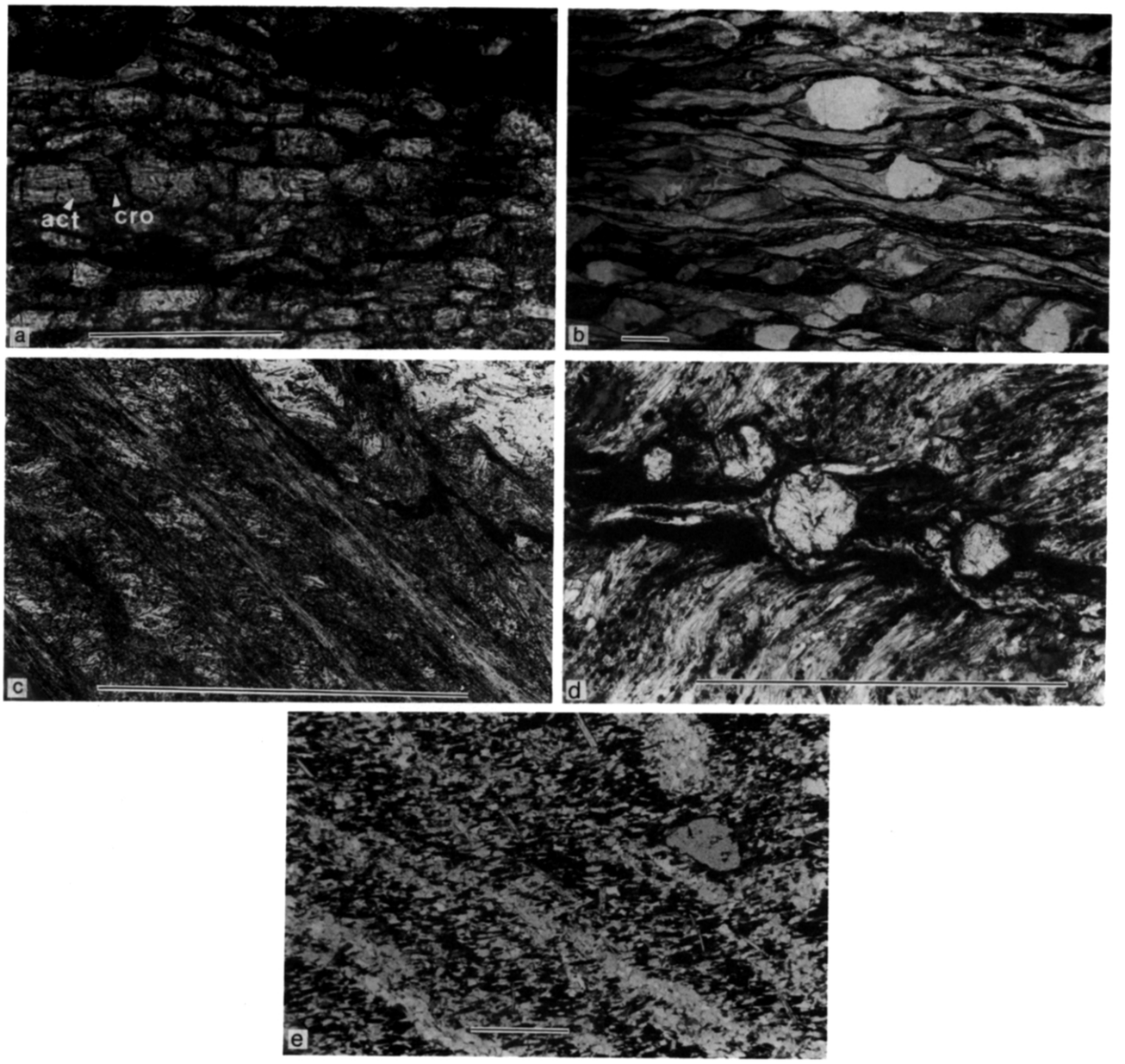

Fig. 12. Microscopic structures and metamorphic textures; all scale bars are 0.5 mm except (a) which is 0.1 mm. (a) D_2 actinolite (act) extended in S_2, displays new growth of fibrous, crossitic amphibole (cro) in the boudin necks, illustrating the stable coexistence of sodic and calcic amphibole (sample 120). (b) Syn-D_3 σ-clasts of pink chert with recrystallized quartz tails illustrate the non-coaxial nature of S_3. (c) S_3 actinolite overgrowth crenulated S_2 crossite (sample 101). (d) Discrete, S_5, fracture solution cleavage is accompanied by new growth of fine-grained muscovite and corrodes D_4 garnet (sample 90). (e) Close to the boundary with the Tia Granodiorite, all biotite, muscovite and quartz grains are oriented parallel S_5 (E–W in photograph), even those which occur along S_3 or S_4 (NW–SE in photograph) reflecting penetrative, D_5, dynamic recrystallization of the entire rock (sample 25).

sample 101, GR 826205), actinolite contains cores of crenulated, D_2 crossite (Fig. 12c).

In the southern Tia Complex, narrow D_3 mylonite zones are texturally comparable to, although finer-grained (<30 μm) than, S_3 described above. Elsewhere, S_3 is restricted to the hinge zones of tight F_3 folds, where it occurs as a variably developed, zonal crenulation cleavage associated with seams of opaques and some new growth of white mica, chlorite ± epidote in mica schist and actinolite, chlorite, epidote and possibly minor sodic amphibole (sample 13579) in metabasite.

Stable D_3 mineral assemblages in the southern Tia Complex include white mica–chlorite–albite–quartz ± epidote in metasediment and actinolite–chlorite–epidote ± sodic amphibole in metabasite. Due to overprinting thermal metamorphism further north, it is hard to assess what minerals were stable during D_3 other than biotite–muscovite in metasediment and hornblende–brown biotite in metabasite.

D_4 *deformation*

In the lower-grade areas, S_4 is generally a discrete crenulation cleavage defined by seams of opaque material enhanced by the new growth of minor muscovite and chlorite (length <300 μm) in mica schist, and fine actinolite needles, chlorite ± epidote ± green biotite in metabasite. In mica schist in the higher-grade areas, the S_4 crenulation cleavage becomes zonal, in which a fine-grained S_3 foliation is generally openly folded and overgrown along limb regions by coarser-grained (length <200–500 μm), idioblastic, S_4 biotite and minor muscovite. Individual mica grains along these seams are not necessarily oriented in S_4 (e.g. sample 3) reflecting late syn- or post-D_4 static recrystallization. Fine-grained (<100 μm), idiomorphic, inclusion-free garnet (almandine) crystals are intergrown with, and occur as inclusions in, S_4 biotite. Because garnet blasts have overgrown S_3, are intergrown with S_4 and are wrapped by S_5, they formed during D_4. A similar relationship exists for rare, relic, D_4 andalusite grains (sample 89). Matrix minerals include oligoclase and quartz in the highest grade zones. S_4 in metabasite is generally weakly developed and restricted to new growth of prismatic, coarse-grained (length <1500 μm) hornblende which occurs as isolated, individual crystals overgrowing fibrous S_3 hornblende (e.g. sample 88).

D_4 metamorphic grades increase towards the Tia Granodiorite, and D_4 assemblages include biotite–muscovite–albite–quartz–almandine (metasediment) in the transition zone, and biotite–muscovite–oligoclase–quartz–almandine ± andalusite (metasediment) and hornblende–andesine (metabasite) in the highest-grade zones.

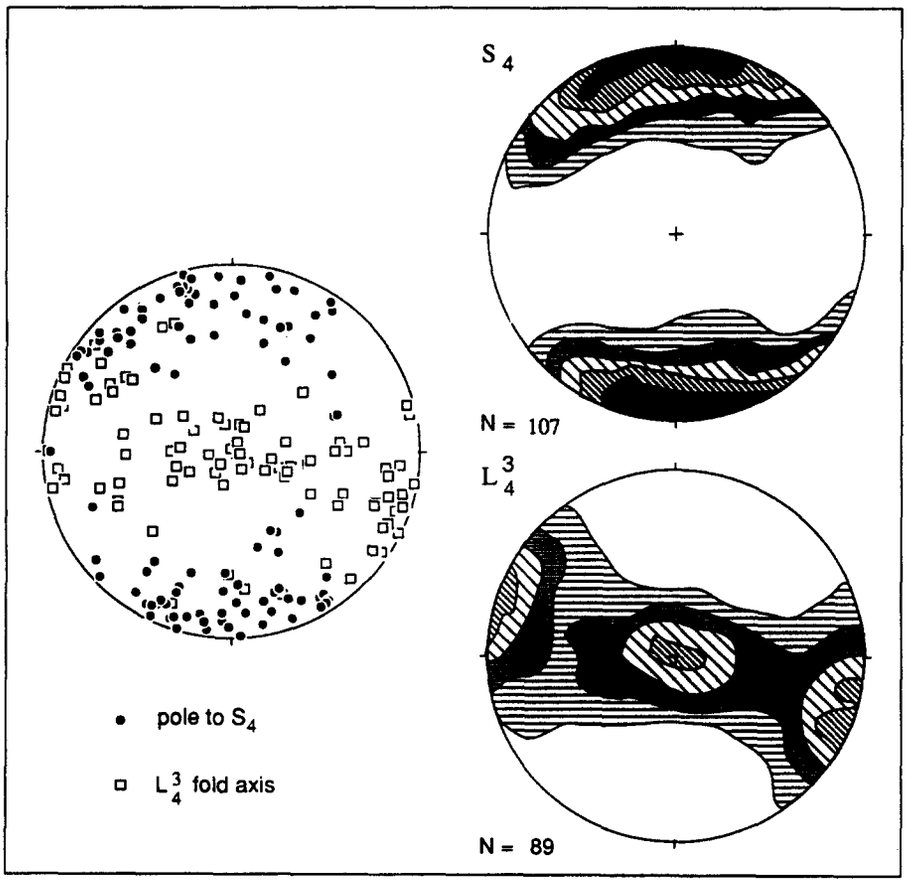

Fig. 9. Equal-area and contour plots of the poles to S_4 and the F_4 fold axes (L_4). The spread of S_4 is mainly due to F_6, whereas the homogeneous spread of L_4 in S_4 reflects cylindrical F_5 folding (see text for further explanation). Contour intervals are 5%.

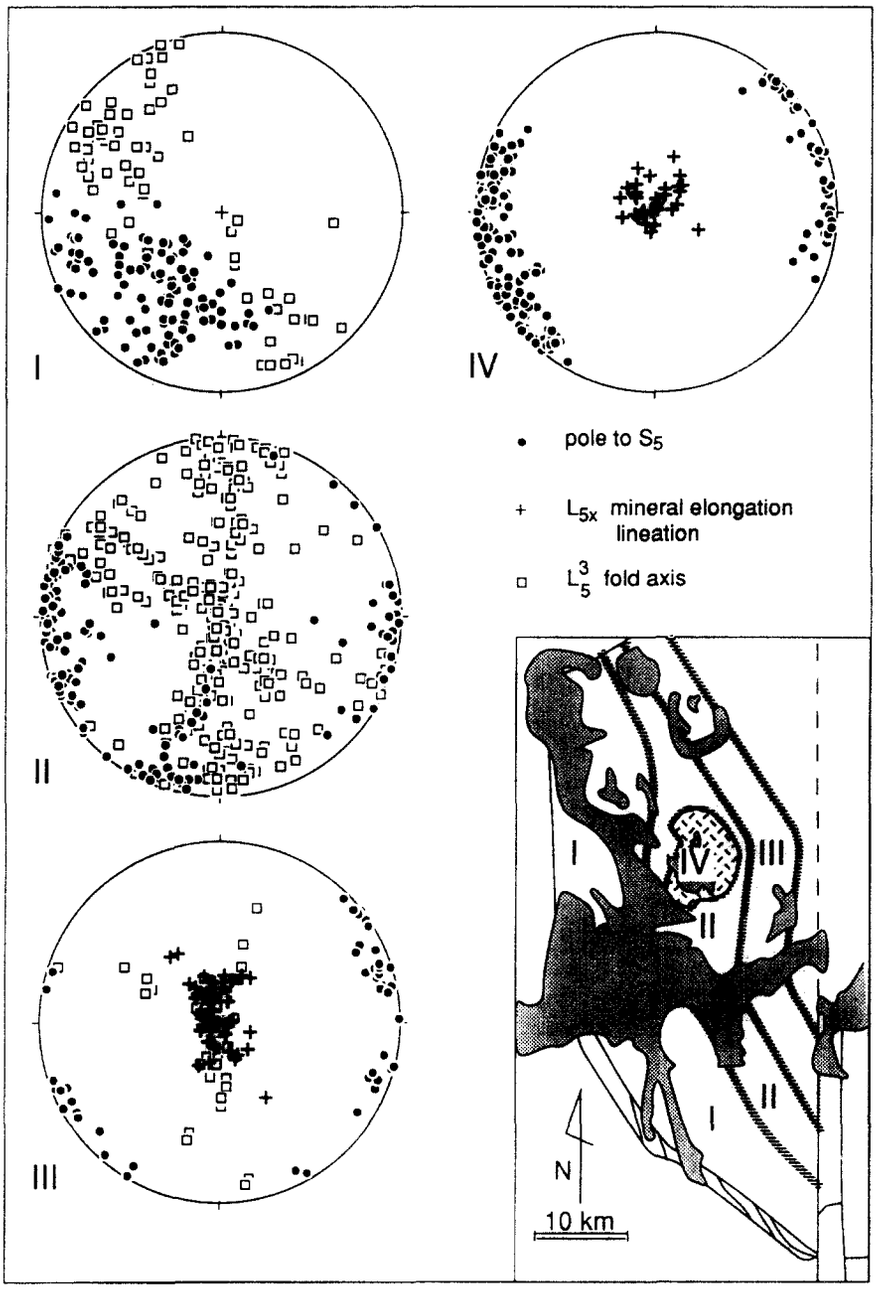

Fig. 10. Equal-area plots of the poles to S_5, the L_{5x} mineral elongation lineation and the F_5 fold axes (L_5) in the four D_5 intensity domains as defined in the text. See text for further discussion on the various distribution patterns.

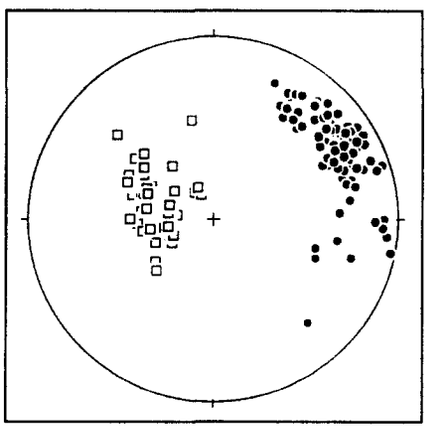

Fig. 11. Equal-area plots of the poles to S_7 (dots) and the L_{7x} (squares) mineral elongation lineation in the Tia Granodiorite. Notice that the spread of S_5 is far less than the spread of S_5 in Fig. 10.

D_5 *deformation*

S_5 in *Domain 1* (Fig. 10) is a discrete solution–crenulation cleavage in quartzitic and metabasic units outlined by seams of opaques. In micaceous rocks, S_5 can be a discrete or zonal crenulation cleavage with minor new growth of fine-grained (<50 μm) chlorite and white mica. In F_5 fold hinges, quartz grains commonly display a grain shape fabric along S_5. As Domain 2 is approached, the discrete fracture solution cleavage is accompanied by new growth of progressively coarser-grained muscovite, chlorite and eventually biotite, whereas D_4 garnet is corroded (e.g. sample 90, Fig. 12d). Likewise, quartz grain shape fabrics which parallel S_5, become more pronounced as the matrix, quartz–mica grain size increases from <50 to <200 μm, reflecting recrystallization of the quartzitic domains. Metabasic rocks have not been observed within the transition zone.

Domain 2 shows effects of syn-deformational contact metamorphism. As the granodiorite is approached quartz and mica domains are progressively recrystallized as all biotite–muscovite grains become oriented in S_5, even those which occur along S_3 or S_4 mica seams (e.g. sample 25, Fig. 12e), and mica grain sizes increase to 300–600 μm. In the vicinity of the Tia Granodiorite, K-feldspar occurs in the matrix (Gunthorpe 1970) and poorly oriented muscovite blasts (length <2000 μm) overgrow S_5 mica grains, though locally, in more intensely developed S_5 cleavage domains, they are enveloped in S_5. Similar relationships exist with euhedral, inclusion free, D_5, almandine–spessartine garnet grains, which only occur within 300 m of the granodiorite contact, and are generally nucleated on D_4 garnet, which may be outlined by circular inclusion trails of quartz.

In *Domain 3*, S_5 is strongly developed, evenly foliated and defined by biotite and muscovite in metasediment, and by fibrous hornblende (length <300 μm) and plagioclase in metabasite. Intrafolial folds and shear band cleavages outlined by finer-grained mica grains are common and illustrate the non-coaxial nature of the fabric. In some metabasic rocks directly east of the granodiorite, S_5 hornblende wraps around domains of variably imbricated, coarse-grained (<1500 μm) hornblende of D_3 or D_4 origin; diopside may be present. Staurolite has been reported from Domain 3 (Gibbons 1989) although the exact location and structural position is unknown.

S_5 in the Tia Granodiorite (*Domain 4*) is generally weak and defined by discontinuous stringers of aligned, coarse-grained (1–4 mm), serrated biotite grains, which separate quartzofeldspathic domains that contain strongly undulose quartz, and mildly undulose equant plagioclase (30–35% An) and perthitic microcline. Quartz domains commonly display a grain shape fabric, whereas feldspar grains are weakly aligned in S_5 and display some recrystallization along their grain boundaries. No primary muscovite appears to have formed during the emplacement of the granodiorite.

Stable mineral assemblages in the highest-grade, D_5 areas include quartz–oligoclase, K-feldspar–biotite–muscovite–garnet (metasediments) and hornblende–plagioclase–diopside (metabasite), whilst migmatitic structures occur on the very edge of the granodiorite (e.g. GR 763515).

D_6, D_7 *and* D_8 *deformation*

Unequivocal D_6 microstructures have not been found. Clear-cut D_7 microstructures are restricted to the Tia Granodiorite. S_7, is defined by narrow (<1 mm), but distinct zones which contain crystallographically aligned, fine-grained (<1 mm) muscovite and biotite, and strongly undulose, dynamically recrystallized quartz. S_7 bends around feldspar crystals and limited recrystallization of plagioclase involving new growth of oligoclase (An ±20%) occurs. S_5 biotite grains are generally dragged into S_7, and are strongly undulose, lozenge-shaped and partly replaced by muscovite and brown biotite.

D_8 effects are restricted to a number of pseudotachylyte veins and associated fracture zones. Where the latter transect quartz veins, they are associated with limited dynamic recrystallization of quartz.

TECTONIC IMPLICATIONS OF THE STRUCTURAL–METAMORPHIC HISTORY

Timing of the structural–metamorphic events

Available Rb/Sr and K/Ar data from the Tia Complex provide most of the age constraints for the area. Many of the dates are mineral ages that do not necessarily date the deformational events during which the mineral formed but rather the time at which a closing temperature for a certain isotope system was passed.

Watanabe *et al.* (1988) dated samples from the southern Tia Complex, and obtained K/Ar ages of 312.3 ± 6 Ma and 318.5 ± 9.3 Ma for white micas (phengite ?) from a chlorite schist (GR 870_5106_5) and a sodic amphibole schist (GR 897_5115), respectively, which were interpreted as the age of high-P metamorphism. Both samples were collected from outcrops where S_2 is the form surface and little new growth of S_3, S_4 and S_5 micas had occurred. The dates probably approximate the age of the S_2 foliation because syn-D_4, peak-metamorphic temperatures in this area were 350–400°C (Hand 1988a, see below), close to the blocking temperature for Ar diffusion in phengitic white mica (310–410°C; Purdy & Jaeger 1976, Sisson & Onstott 1986, Schermer *et al.* 1990).

A K/Ar date of 311 ± 3 Ma was obtained from phengitic white mica from a D_3 mylonite zone (GR 863126; Dirks & Offler unpublished data) in the low-grade part of the complex. Therefore, the date probably approximates the age of D_3.

D_5 deformation was coeval with the emplacement of the Tia Granodiorite. A combination of several plutons including the Tia Granodiorite, provided Rb/Sr whole

rock isochron ages of 295 ± 25 Ma (Flood & Shaw 1977) and 312 ± 12 Ma (Hensel 1982), which were interpreted to approximate the emplacement age of the Hillgrove Suite (Hensel *et al.* 1985). Watanabe *et al.* (1988) recombined their data and obtained a better constrained age of 290 ± 4 Ma. Recent U–Pb ages from magmatic zircon from the Tia Granodiorite yield well constained ages of ~300 Ma (Collins & Offler unpublished data). Considering the *S*-type nature of these granites (Flood & Shaw 1977, Shaw & Flood 1981), which suggests emplacement shortly after magma generation, and the high blocking temperature for U–Pb systems in zircon, it appears that 300 Ma approximates the age of granite emplacement and thus D_5.

Rb/Sr biotite data obtained from two samples of Tia Granodiorite (GR 798493 and GR 802545) give model ages of 264 ± 1.3 Ma and 262 ± 1.3 Ma (Dirks *et al.* in press b) assuming a $^{87}Sr/^{86}Sr$ ratio of 0.706 (Watanabe *et al.* 1988). As the Rb/Sr blocking temperature for biotite is 320 ± 40°C (Harrison & McDougall 1980), the dates record cooling from the metamorphic peak. Since biotite was stable in the granodiorite during D_7 but not during D_8, 260 Ma probably reflects uplift during D_7 and D_8 (Dirks *et al.* in press a).

Pressure–temperature estimates

D_1 assemblages are incomplete and *P–T* estimates are tentative. However, the possible occurrence of lawsonite + quartz, now replaced by albite ± pumpellyite ± epidote, the coexistence of sodic and calcic amphiboles rather than barroisite (Ernst 1979), and the jadeitic rims on mafic pyroxene (X_{jd} = 0.25), indicate conditions of 200–250°C and 6–6.5 kbar (Hand 1988a; using the ideal sodic pyroxene mixing model of Essene & Fyfe 1967, and the Al_2O_3 content in sodic amphibole, Maruyama *et al.* 1986).

During D_2, the apparent stable coexistence of pumpellyite, actinolite and epidote (Nitsch 1971, Liou *et al.* 1985), the coexistence of sodic amphibole, calcic amphibole and epidote (Brown 1977), and the absence of sodic pyroxene are all indicative of pressure–temperature conditions of approximately 280–320°C and 5.5–6 kbar (Hand 1988a; using Fe/Mg ratios in coexisting chlorite–actinolite, Cho M. in Laird 1988, and the Al_2O_3 content in sodic amphibole, Maruyama *et al.* 1986).

In the lower-grade, southern Tia Complex, S_3 as compared to S_2 white mica is generally enriched in paragonite and celadonite (Hand 1988a) reflecting an increase in temperature and possibly a decrease in pressure (Guidotti & Sassa 1976, Massone & Schreyer 1983). The limited new growth of S_3 sodic amphibole, and the generally observed replacement of sodic amphibole by actinolite, suggests that intermediate pressures (3–5 kbar) prevailed during D_3, as the terrain moved from blueschist to greenschist facies conditions. In the higher-grade parts of the complex, biotite and hornblende assemblages indicate temperatures in excess of 400°C (e.g. Yardley 1989). Towards the northeast, pressures are expected to be progressively lower, because S_3 is essentially a mylonitic fabric recording a southwest-up sense of movement.

During D_4 in the southern Tia Complex, sodic amphiboles and pumpellyite are no longer stable, and green biotite formed in metabasite, but not in metapelite. This suggests D_4 conditions shifted well into the greenschist facies at temperatures of 350–400°C and pressures of less than 4 kbar (e.g. Yardley 1989). Using Fe/Mg ratios in coexisting chlorite–actinolite pairs a pressure estimate of 2–3 kbar could be derived (Hand 1988a, Laird 1988). D_4 assemblages in the higher-grade areas, in which muscovite + quartz is stable and andalusite is present, indicate that amphibolite facies conditions were attained with maximum temperatures of ~550–600°C and pressures of between 1.5 and 3.5 kbar (Turner 1981). This is consistent with the observation that during D_4 and subsequent events the Tia Complex behaved as a relatively coherent unit, so that pressure estimate of 2–3 kbars from the southern Tia Complex should be similar to the pressure conditions further north.

Peak D_5 assemblages and limited migmatization of the metapelitic rocks at the granodiorite boundary, are indicative of upper amphibolite grade conditions with temperatures of 600–650°C. The presence of staurolite and stable quartz + muscovite, and the absence of magmatic muscovite in the granodiorite suggest pressures of 2–3 kbar (Harte & Hudson 1979, Zen 1988). Because D_5 was associated with uplift of the Tia Complex on the eastern thrust, pressures are expected to be slightly less than during D_4.

Since no D_6 assemblages have been found, *P–T* conditions are hard to estimate. D_6 presumably coincides with the opening of Permian extensional basins, and heat flow is expected to be high. The presence of blueschist fragments in the basal conglomerates of the Wards Creek formation (GR 778093), in the Manning Basin directly south of the Tia Complex, suggests that blueschist from the southern Tia Complex was at the surface during late D_5–D_6.

The retrograde D_7 association biotite–muscovite–oligoclase in the granodiorite, suggests that conditions were still at amphibolite grade with temperatures of ~500–600°C. There is no indication that retrogression occurred prior to D_7 and it appears that D_{4-7} are associated with one extended thermal event. The D_8 brittle fracture zones, which probably evolved from D_7, show limited dynamic recrystallization of quartz, suggesting they formed at the brittle–ductile transition for quartz.

Kinematic history

The D_1 structures noted in the rocks from the Tia Complex, are typical for accretionary sequences (e.g. Fergusson 1984, Mackenzie *et al.* 1987, Needham & Mackenzie 1988) and may reflect the results of various stages of non-coaxial deformation, which caused brecciation, stratal disruption (asymmetric, phacoidal fabrics) and burial of the rocks to depths where blueschist facies conditions existed during the development of S_1 and S_2 (Mackenzie *et al.* 1987, Hand 1988a).

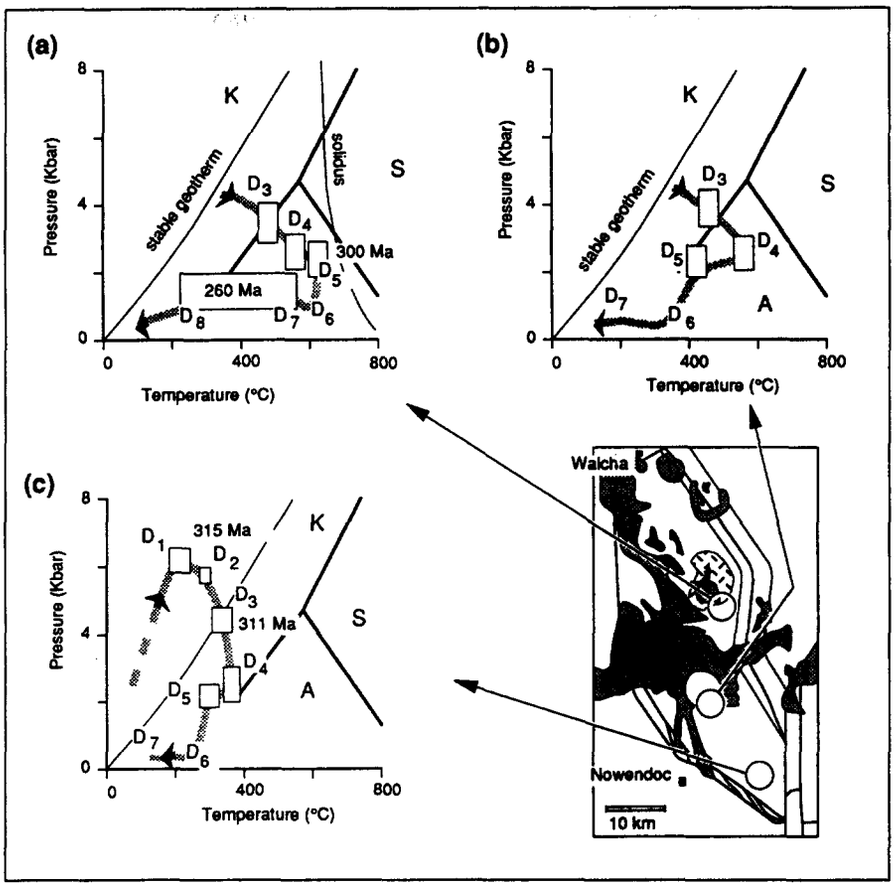

Fig. 13. *P–T–t*-deformation, summary diagram for (a) the central Tia Complex which underwent maximum heating, (b) the transition zone from thermally perturbed rocks to the rocks with high-*P* assemblages and (c) rocks that preserved high-*P* asemblages. The aluminium triple point used in this diagram is the thermodynamically calculated value of Powell & Holland (1988, 4.5 kbar, 570°C). The stable geotherm is based on heat flow measurements in Proterozoic basement with normal thickness crust (e.g. Loosveld & Etheridge 1990). See text for further discussion.

S_2 is a shallowly SW-dipping, non-coaxial, blueschist fabric that records a normal sense of movement. Because S_2 is only preserved in the hanging wall of a D_3 thrust and may have undergone major body rotations, it is doubtful if this orientation represents the original position of S_2.

D_3 structures present a better constrained kinematic picture. S_3 in most of the complex is mylonitic in nature, and although the shear strain could not be measured, the intensity of S_3 suggests it was large. In the western half of the complex, where later deformation was weak, S_3 dips moderately WSW, and the movement sense is consistently W-over-E along a down-dip lineation. This is consistent with the NE-vergence of the antiformal F_3 structure east of Nowendoc, which probably represents a hanging wall antiform. Cross-sections indicate that the non-coaxial D_3 zone is at least 10 km thick (Fig. 4), which suggests that major uplift of the hanging wall occurred.

East-over-west movement also occurred during D_5 and D_7, although it was restricted to distinct, steeply W-dipping shear zones, above which the Tia Complex was coherently uplifted. Metamorphic grades stayed within the biotite stability field from D_5 to D_7, whereas grades drop sharply across the D_5 high strain zone (Domain 3). This suggests that juxtaposition of the metamorphic terrains occurred during D_{7-8}, on a shear zone that parallels the D_5 shear zone (Figs. 4, 5 and 6).

Throughout most of its history, from D_3 to D_8, the fabrics in the Tia Complex record W-over-E movement on W-dipping shears in a mainly E–W compressional regime. Only during D_6, when quartz veins appear to have been formed along steeply W-dipping surfaces that record a W-down sense of movement, did this kinematic picture change. This coincides with a relatively long time interval (300–260 Ma) when the Permian Basins developed (Leitch 1988), and little penetrative deformation was recorded in the rocks.

The history as presented above can be summarized in a *P–T–t*-deformation diagram (Fig. 13) which illustrates the clockwise nature of the *P–T* path connecting two extremely dissimilar *P–T* domains. D_{1-2} are associated with anomalously high-*P*, low-*T*, conditions, whereas conditions during D_{4-5}, and probably D_6 and D_7, are associated with anomalously high-*T*, low-*P*. This raises a number of important questions regarding the tectonic evolution and uplift history of the Tia Complex:

(1) What process induced the uplift from D_1 to D_5?

(2) What is the significance of the high heat flow during D_{4-7} in terms of uplift history and tectonic setting, and why was it maintained for ~40 Ma (300–260 Ma)?

(3) Where do the fault-bounded, extensional, Permian Basins fit into this tectonic story?

Terrains similar to the Tia Complex occur elsewhere in the NEFB. For example, in the Wongwibinda Complex, where only an anomalously high temperature assemblage has been preserved (Farrell 1988) associated with Hillgrove Suite plutons, and in the D'Aguilar Block west of Gympie (Queensland), where the situation is similar to Tia with blueschist, high-T amphibolites, 300 Ma granite plutons, a 250–260 Ma cooling age and a faulted contact with the Permian Esk Rift sequence (Holcombe *et al.* 1990). This suggests that the high-T events occur along a N–S belt, parallel to the trend of the New England orogen.

DISCUSSION AND CONCLUSIONS

Rocks in the Tia Complex underwent a simple clockwise P–T–t-deformation path and moved from mid-crustal levels at blueschist facies conditions (D_{1-2}, ~6 kbar–200°C) to upper-crustal levels at high-T amphibolite facies conditions (D_{4-5}, ~2.5 kbar–600°C) in a relatively short time (~15 Ma, Fig. 13). The rocks remained under these conditions for ~40 Ma (D_6) before they cooled and were finally brought to the surface (D_{7-8}). During this period, Permian rift basins were opening as thermal gradients in the Tia Complex reached a maximum (Fig. 13). There is little information as to when the Permian Basins first opened, but the lowermost unit of the Manning Basin (the Wards Creek Formation, Mayer 1972) is older than early Permian and possibly late Carboniferous based on fossil assemblages (Mayer 1972, Leitch 1988, Briggs 1991). This suggests that the first extensional basins opened during D_{4-5} as compression and heating was going on at the 2–3 kbar level. Extension of the basins continued until ~266 Ma (Briggs 1991, Collins 1991): after that compression occurred which coincided with the final cooling and uplift of the terrain.

The early, pre-D_1 to D_2 history of the Tia Complex was associated with accretion–subduction processes such as progressive tilting of the foliations, disruption of bedding, melange formation and blueschist facies metamorphism, similar to other terrains in the New England orogen (e.g. Fergusson 1984, Cross *et al.* 1987, Fergusson *et al.* 1990). The later, D_{3-7} uplift and thermal history cannot be directly related to accretion–subduction processes. D_{3-7} uplift of the Tia Complex occurred in response to compression (thrusting) and erosional denudation, and was at a maximum during D_3 when a sharp rise in geothermal gradients occurred that must have resulted in heating and weakening of the lithosphere. Uplift practically stopped as geothermal gradients reached a maximum and extensional basins opened, but continued again after the terrain cooled during D_7.

The shift from subduction-related to thermal processes occurred during D_{3-4} uplift of at least 3–4 kbar (~10–15 km) around 300–310 Ma (Fig. 13). This shift roughly coincided with the termination of the NNW-trending volcanic arc 100 km west of the Tia Complex and the initiation of a new arc to the east, incorporating the Gympie Volcanics of southeast Queensland (Day *et al.* 1978, Harrington & Korsch 1985, Waterhouse & Sivell 1987, Murray 1990). It suggests that subduction associated with the accretion of the Tableland Complex stopped (Murray *et al.* 1987) as the locus of subduction shifted east (Waterhouse & Sivell 1987, Murray 1990). Thus, during D_{3-5}, the Tia Complex changed its tectonic setting from an accretionary prism to a back-arc position in which it was directly overlying the remains of a subducted slab. The terrain essentially remained in compression, probably because convergent subduction processes continued farther east.

In its back-arc position, the Tia Complex was heated and remained anomalously hot for close to 40 Ma (Dirks *et al.* in press a) (Fig. 13). A possible explanation for the inferred high crustal temperatures is that they resulted from convective heat input due to the emplacement of the plutons of the Hillgrove and Bundara Suites (Vernon 1982). However, in this way high temperatures cannot be maintained for very long (<5 Ma) unless very large volumes of granite are continually emplaced in the crust (e.g. Loosveld & Etheridge, 1990). Since no large volumes of granite are associated with the high-temperature metamorphics in the Tia Complex, a more fundamental disturbance of the lithospheric thermal structure must have existed. It is generally thought that this requires removal of the mantle lithosphere, so that the asthenosphere can come in direct contact with the lower crust (e.g. Loosveld & Etheridge 1990, Sandiford & Powell 1991). Underneath the Tableland Complex removal of the mantle lithosphere may be achieved if detachment of the subducting slab occurred after subduction stopped in the late Carboniferous and the remaining slab became gravitationally unstable. The duration of the metamorphic event may reflect the time it took for the subducted slab to thermally re-equilibrate.

Heating of the crust underlying the Tia Complex must have resulted in thermal doming and uplift as the crust itself weakened. This may explain the shift in the upper crust from a compressional to an extensional situation as the Permian Basins opened around 300 Ma; a situation that was maintained for as long as high heat flows and thermal doming affected the area.

Acknowledgements—Work was supported by an Australian Research Council grant No. A38930121 to Drs Collins and Offler. We wish to thank Bill Landenberger and Terry Farrell for helpful discussions on the Tia Complex and related terrains, and Tim Needham and an anonymous referee for their critical comments which helped improve this paper.

REFERENCES

Binns, R. A. 1966. Granitic intrusions and regional metamorphism of Permian age from the Wongwibinda Complex, northeastern New South Wales. *J. Proc. R. Soc. NSW* **99**, 5–36.

Briggs, D. J. C. 1991. Correlation charts for the Permian of the Sydney–Bowen Basin and the New England Orogen. *Advances in*

the Study of the Sydney Basin, Proceedings of the 25th Symposium, Newcastle, 30–37.

Brown, E. H. 1977. The crossite content of Ca-amphibole as a guide to the pressure of metamorphism. *J. Petrol.* **18**, 53–72.

Cawood, P. A. & Leitch, E. C. 1985. Accretion and dispersal tectonics of the Southern New England Fold Belt, eastern Australia. In: *Tectonostratigraphic Terrains of the Circum-Pacific Region* (edited by Howell, D. G.). *Circum-Pacific Council for Energy and Mineral Resources, Earth Sci. Ser.* **I**, 481–492.

Cobbold, P. R. & Quinquis, H. 1980. Development of sheath folds in shear regimes. *J. Struct. Geol.* **2**, 119–126.

Collins, W. J. 1991. A reassessment of the 'Hunter–Bowen Orogeny': tectonic implications for the Southern New England Fold Belt. *Aust. J. Earth Sci.* **38**, 409–423.

Cross, K. C., Fergusson, C. L. & Flood, P. G. 1987. Contrasting structural styles in the Paleozoic subduction complex of the southern New England Orogen, eastern Australia. In: *Terrane Accretion and Orogenic Belts* (edited by Leitch, E. C. & Scheiber, E.). *Am. Geophys. Un., Geodyn. Ser.* **19**, 83–92.

Day, R. W., Murray, C. G. & Whitaker, W. G. 1978. The eastern part of the Tasman Orogenic Zone. *Tectonophysics* **48**, 327–364.

Dirks, P. H. G. M., Offler, R. & Collins, W. J. In press a. Emplacement and deformation of the Tia Granodiorite, southern New England Fold Belt, NSW; implications for the metamorphic history. *Aust. J. Earth Sci.*

Dirks, P. H. G. M., Lennox, P. G. & Shaw, S. E. In press b. Implications of two Rb/Sr dates for the Tia Granodiorite, southern New England Fold Belt, NSW, Australia. *Aust. J. Earth Sci.*

Ernst, W. G. 1979. Coexisting sodic and calcic amphibolites from high-pressure metabasic belts and the stability of barroisitic amphibole. *Mineralogy Mag.* **43**, 269–278.

Essene, E. J. & Fyfe, W. S. 1967. Omphacite in Californian metamorphic rocks. *Contr. Miner. Petrol.* **15**, 1–23.

Farrell, T. R. 1988. Structural geology and tectonic development of the Wongwibinda Metamorphic Complex. In: *New England Orogen; Tectonics and Metallogenesis, Symposium Proceedings* (edited by Kleeman, J. D.). University of New England, Armidale, 117–124.

Fergusson, C. L. 1984. The Gundahl Complex of the New England Fold Belt, eastern Australia: a tectonic mélange formed in a Palaeozoic subduction complex. *J. Struct. Geol.* **6**, 257–271.

Fergusson, C. L., Henderson, R. A. & Leitch, E. C. 1990. Subduction complex melange of the Wandilla terrane, Palaeozoic New England Orogen, central Queensland, Australia. *J. Struct. Geol.* **12**, 591–599.

Flood, R. H. & Shaw, S. E. 1977. Two 'S-type' granite suites with low initial $^{87}Sr/^{86}Sr$ ratios from the New England Batholith, Australia. *Contr. Miner. Petrol.* **61**, 163–173.

Gibbons, D. 1989. Structure of the northern Tia Granodiorite and surrounding metamorphics. Unpublished B.Sc. (Hons.) thesis, University of New South Wales, Sydney.

Gray, D. R. 1977. Morphological classification of crenulation cleavage. *J. Geol.* **85**, 229–235.

Guidotti, C. V. & Sassi, F. P. 1976. Muscovite as a petrogenetic indicator mineral in pelitic schists. *Neues Jb. Miner. Abh.* **153**, 363–380.

Gunthorpe, R. J. 1970. Plutonic and metamorphic rocks of the Walcha–Nowendoc–Yarrowitch district, New South Wales. Unpublished Ph.D. thesis, University of New England, Armidale.

Hand, M. 1988a. A structural and metamorphic analysis of a highly deformed accretion–subduction sequence, Nowendoc, NSW. Unpublished B.Sc. (Hons.) thesis, University of Newcastle, Newcastle, Australia.

Hand, M. 1988b. Structural analysis of a deformed subduction–accretion complex sequence, Nowendoc, NSW. In: *New England Orogen; Tectonics and Metallogenesis, Symposium Proceedings* (edited by Kleeman, J. D.). University of New England, Armidale, 105–116.

Harrington, H. J. & Korsch, R. J. 1985. Tectonic model for the Devonian to middle Permian of the New England Orogen. *Aust. J. Earth Sci.* **32**, 163–179.

Harrison, T. M. & McDougall, I. 1980. Investigations of an intrusive contact, northwest Nelson, New Zealand—1. Thermal, chronological and isotopic constraints. *Geochim. cosmochim. Acta* **44**, 1985–2003.

Harte, B. & Hudson, N. F. C. 1979. Pelite facies series and the temperatures and pressures of Dalradian metamorphism in E Scotland. In: *The Caledonides of the British Isles—Reviewed* (edited by Harris, A. L., Holland, C. H. & Leake, B. E.). *Spec. Publs geol. Soc. Lond.* **8**, 323–368.

Hensel, H. D. 1982. The mineralogy, petrology and geochronology of granitoids and associated intrusives from the northern portion of the New England Batholith. Unpublished Ph.D. thesis, University of New England, Armidale.

Hensel, H. D., McCulloch, M. T. & Chappell, B. W. 1985. The New England Batholith: constraints on its derivation from Nd and Sr isotopic studies of granitoids and country rocks. *Geochim. cosmochim. Acta* **49**, 369–384.

Holcombe, R. J., Little, T. A., Gibson, G. M., Sliwa, R. & Dobos, S. K. 1990. Structural and metamorphic framework of the north D'Aguillar Block, southeast Queensland. *Proc. Aust. Inst. Min. Met., Pacific Rim Congress* 90 **3**, 173–178.

Korsch, R. J. 1977. A framework for the Palaeozoic geology of the southern part of the New England Geosyncline. *J. geol. Soc. Aust.* **25**, 339–355.

Laird, J. 1988. Chlorites: Metamorphic Petrology. In: *Hydrous Phyllosilicates (Exclusive of Micas)* (edited by Bailey, S. W.). *Mineral. Soc. Am. Rev. Mineral.* **19**, 405–453.

Leitch, E. C. 1988. The Bernard Basin and the early Permian development of the southern part of the New England Fold Belt. In: *New England Orogen: Tectonics and Metallogenesis, Symposium Proceedings* (edited by Kleeman, J. D.). University of New England, Armidale, 61–67.

Liou, J. G., Maruyama, S. & Cho, M. 1985. Phase equilibria and mineral paragenesis of metabasites in low-grade metamorphism. *Mineralog. Mag.* **49**, 321–333.

Loosveld, R. J. H. & Etheridge, M. A. 1990. A model for low-pressure facies metamorphism during crustal thickening. *J. metamorph. Geol.* **8**, 257–267.

Mackenzie, J. S., Needham, D. T. & Ager, S. M. 1987. Progressive deformation in an accretionary complex: an example from the Shimanto Belt of eastern Kyushu, southwest Japan. *Geology* **15**, 353–356.

Maruyama, S., Cho, M. & Liou, J. G. 1986. Experimental investigations of blueschist–greenschist transition equilibria: pressure dependence of Al_2O_3 contents in sodic amphiboles—a new geobarometer. *Mem. geol. Soc. Am.* **164**, 1–16.

Massone, H. J. & Schreyer, W. 1983. A new experimental phengite barometer and its application to a Variscan subduction zone at the southern margin of the Rhenohercynicum. *Terra Cognita* **3**, 1–18.

Mayer, W. 1972. Palaeozoic sedimentary rocks from southern New England: a sedimentological evaluation. Unpublished Ph.D. thesis, University of New England, Armidale.

Morand, V. J. 1982. Structure and metamorphism in the central part of the Tia Complex. In: *New England Geology, Symposium Proceedings* (edited by Flood, P. G. & Runnigar, B. N.). University of New England, Armidale, 95–103.

Murray, C. G., Fergusson, C. L., Flood, P. G., Whitaker, W. G. & Korsch, R. J. 1987. Plate tectonic model for the Carboniferous evolution of the New England Fold Belt. *Aust. J. Earth Sci.* **34**, 213–236.

Murray, C. G. 1990. Comparison of suspect terrains of the Gympie Province with other units of the New England Fold Belt, eastern Australia. *Proc. Aust. Inst. Min. Met., Pacific Rim Congress* 90 **2**, 247–255.

Needham, D. T. & Mackenzie, J. S. 1988. Structural evolution of the Shimanto Belt accretionary complex in the area of the Gokase River, Kyushu, southwest Japan. *J. geol. Soc. Lond.* **145**, 85–94.

Nitsch, K. H. 1968. Die stabilität von Lawsonit. *Naturwissenschaften* **55**, 38.

Nitsch, K. H. 1971. Stabiliotätsbeziehungen von Prehnit- und Pumpellyit-haltiger Paragenesen. *Contr. Miner. Petrol.* **30**, 240–260.

Passchier, C. W. & Simpson, C. 1986. Porphyroclast systems as kinematic indicators. *J. Struct. Geol.* **8**, 831–843.

Powell, R. & Holland, T. J. B. 1988. An internally consistent thermodynamic dataset with uncertainties and correlations: 3. Applications to geobarometry, worked examples and a computer program. *J. metamorph. Geol.* **6**, 173–204.

Purdy, J. W. & Jaeger, E. 1976. K-Ar ages on rock forming minerals from the Central Alps. *Mem. Inst. Geol. Mineral. Univ. Padova* **30**, 1–31.

Ramsay, J. G. 1967. *Folding and Fracturing of Rocks*. McGraw-Hill, New York.

Ramsay, J. G. & Huber, M. I. 1987. *The Techniques of Modern Structural Geology, Volume 2: Folds and Fractures*. Academic Press, London.

Runnegar, B. N. 1974. The geological framework of New England. *Geol. Soc. Aust., Qld Div., Field Conference of the New England Area*, 9–19.

Sandiford, M. 1989. Horizontal structures in granulite terrains: a record of mountain building or mountain collapse? *Geology* **17**, 449–452.

Sandiford, M. & Powell, R. 1991. Isostatic and thermal constraints on the evolution of high temperature–low pressure metamorphic terrains in convergent orogens. *J. metamorph. geol.* **9**, 333–340.

Schermer, E. R., Lux, D. R. & Clark Burchfiel, B. 1990. Temperature–time history of subducted continental crust, Mount Olympos region, Greece. *Tectonics* **9**, 1165–1195.

Shaw, S. E. & Flood, R. H. 1981. The New England Batholith, eastern Australia: geochemical variations in time and space. *J. geophys. Res.* **86**, 10,530–10,544.

Sisson, V. B. & Hollister, L. S. 1988. Low-pressure facies series metamorphism in an accretionary sedimentary prism, southern Alaska. *Geology* **16**, 358–361.

Sisson, V. B. & Onstott, T. C. 1986. Dating blueschist metamorphism: a combined $^{40}Ar/^{39}Ar$ and electron microprobe approach. *Geochim. cosmochim. Acta* **50**, 2111–2117.

Stern, T. A. 1987. Asymmetric back-arc spreading, heat flux and structure associated with the Central Volcanic Region, New Zealand. *Earth Planet. Sci. Lett.* **85**, 265–276.

Thiessen, R. L. & Means, W. D. 1980. Classification of fold interference patterns: a reexamination. *J. Struct. Geol.* **2**, 311–316.

Turner, F. J. 1981. *Metamorphic Petrology*. McGraw-Hill, New York.

Vernon, R. H. 1982. Isobaric cooling of two regional metamorphic complexes related to igneous intrusions in southeastern Australia. *Geology* **10**, 76–81.

Watanabe, T., Iwasaki, M., Ishiga, H., Ilizumi, S., Honma, H., Kawachi, Y., Morris, P., Naka, T. & Itaya, T. 1988. Late Carboniferous Orogeny in the southern New England Fold Belt, NSW, Australia. In: *New England Orogen: Tectonics and Metallogenesis, Symposium Proceedings* (edited by Kleeman, J. D.). University of New England, Armidale, 93–98.

Waterhouse, J. B. & Sivell, W. J. 1987. Permian evidence for trans-Tasman relationships between east Australia, New Caledonia and New Zealand. *Tectonophysics* **142**, 227–240.

Yardley, B. W. D. 1989. *An Introduction to Metamorphic Petrology*. Longman Scientific & Technical, Harlow.

Zen, E-an. 1988. Phase relations of peraluminous granitic rocks and their petrogenetic implications. *Annu. Rev. Earth & Planet. Sci.* **16**, 21–51.